

Available online at www.sciencedirect.com

journal homepage: www.elsevier.com/locate/ajps

Original Research Paper

A multi-functional nanoplatform for efficacy tumor theranostic applications

Jinjin Shi, Hongling Zhang, Zhaoyang Chen, Lihua Xu, Zhenzhong Zhang *

School of Pharmaceutical Sciences, Zhengzhou University, Zhengzhou, China

ARTICLE INFO

Article history:

Received 30 August 2016

Received in revised form 22

November 2016

Accepted 7 December 2016

Available online 21 December 2016

Keywords:

Multifunctional drug delivery

Endosome escape

Tumor-targeting

Bio-imaging

Theranostic

ABSTRACT

Nanomaterials with multiple functions have become more and more popular in the domain of cancer research. MoS₂ has a great potential in photothermal therapy, X-ray/CT imaging and drug delivery. In this study, a water soluble MoS₂ nanosystem (MoS₂-PEG) was synthesized and explored in drug delivery, photothermal therapy (PTT) and X-ray imaging. Doxorubicin (DOX) was loaded onto MoS₂-PEG with a high drug loading efficiency (~69%) and obtained a multifunctional drug delivery system (MoS₂-PEG/DOX). As the drug delivery, MoS₂-PEG/DOX could efficiently cross the cell membranes, and escape from the endosome via NIR light irradiation, lead to more apoptosis in MCF-7 cells, and afford higher antitumor efficacy without obvious toxic effects to normal organs owing to its prolonged blood circulation and 11.6-fold higher DTX uptake of tumor than DOX. Besides, MoS₂-PEG/DOX not only served as a drug delivery system, but also as a powerful PTT agent for thermal ablation of tumor and a strong X-ray contrast agent for tumor diagnosis. In the *in vitro* and *in vivo* studies, MoS₂-PEG/DOX exhibited excellent tumor-targeting efficacy, outstanding synergistic anti-cancer effect of photothermal and chemotherapy and X-ray imaging property, demonstrating that MoS₂-PEG/DOX had a great potential for simultaneous diagnosis and photothermal-chemotherapy in cancer treatment.

© 2017 Production and hosting by Elsevier B.V. on behalf of Shenyang Pharmaceutical University. This is an open access article under the CC BY-NC-ND license (<http://creativecommons.org/licenses/by-nc-nd/4.0/>).

1. Introduction

The ultimate goal of cancer therapeutics is to increase the survival time and the life quality of the patient by reducing the unintended harmful side-effects [1]. Although, the medical science and biomedical engineering advanced to a significant extent, the therapeutic development of anti-cancer

strategies is often limited by administration problem of the drugs [2]. In recent years, with the development of cancer nanotechnology, researchers have focused on developing nanoscale anticancer drug carriers for improving therapeutic efficacy as well as reducing unwanted side effects [3–5]. Research on graphene highlights a new two-dimensional (2D) nanosystem in the area of biomedicine [6–8], just like graphene, layered molybdenum disulfide (MoS₂) is another 2D nanostructure [9,10].

* Corresponding author. School of Pharmaceutical Sciences, Zhengzhou University, Zhengzhou, China. Fax: +86 371 67781908.

E-mail address: zhangzz08@126.com (Z. Zhang).

Peer review under responsibility of Shenyang Pharmaceutical University.

<http://dx.doi.org/10.1016/j.ajps.2016.12.001>

1818-0876/© 2017 Production and hosting by Elsevier B.V. on behalf of Shenyang Pharmaceutical University. This is an open access article under the CC BY-NC-ND license (<http://creativecommons.org/licenses/by-nc-nd/4.0/>).

MoS₂ is composed of two layers of sulfur atoms and a layer of molybdenum atoms, and a layer of molybdenum atoms is sandwiched between the two layers of sulfur atoms [11-13]. Compared with graphene, MoS₂ has many similar electronic, optical, mechanical and chemical properties, making it have a great potential in the area of biomedicine [14]. Graphene had been successfully explored its applications as biosensors, photothermal agents, drug delivery platforms, and tissue engineering scaffolds [12,15]. The success of graphene encouraged the exploration of MoS₂ for biomedical applications. So far, there are only a few reports using MoS₂ in the area of biomedicine, especially in cancer diagnosis and treatment applications. Liu et al. used PEGylated MoS₂ as a multifunctional theranostic agent for *in vivo* dual modal CT/photoacoustic imaging guided photothermal therapy, and achieved a good tumor theranostic efficacy [16]. However, the above system did not explore the application of MoS₂ as an antitumor drug delivery platform, and the biological safety of MoS₂ *in vivo* had not been explored to our best knowledge.

MoS₂ has a huge specific surface area, high thermal and chemical stability, and the surface layers of sulfur atoms make MoS₂ have a good adsorption capacity to small molecules [17]. The above properties give MoS₂ great advantages as a drug delivery platform. However, the inherent hydrophobicity limit its use in biology and thus lead to the research in searching water-soluble MoS₂ derivatives [18]. For drug delivery applications, PEGylation has been widely used to extend the circulation time of a drug system, allowing the drug more time to accumulate in the tumor via the enhanced permeability and retention effect [19,20]. So in this study, PEG-modified MoS₂ was used to explore its applications in drug delivery.

Photothermal therapy (PTT) uses light absorbing agents to convert optical energy into heat, leading to the thermal ablation of cancer cells [21,22]. In recent years, PTT as a minimally invasive, controllable, and highly efficient treatment method has drawn widespread attention. MoS₂ nano sheets exhibit strong visible to NIR absorbance owing to the surface plasmon resonance (SPR) effect, making it powerful agents in PTT cancer treatment [21]. In this study, we hypothesized that exposure to a focused external NIR light (808 nm) would lead to significant heat release by the functionalized MoS₂, allowing it to serve directly as an anticancer therapeutic agent.

Another advantage of MoS₂ is its novel X-ray imaging ability [23,24]. X-ray computed tomography is widely used for screening and diagnosis of various pathologies including cancer. The ability to visualize deep structures in the body is the main advantage of X-ray imaging. Just like gold, molybdenum also has a high atomic number and a high absorption coefficient giving MoS₂ great contrast per unit weight [24]. In this study, MoS₂ was also used as a X-ray imaging contrast agent for tumor diagnosis.

An ideal drug delivery system should not only accumulate drugs in tumor tissue, enter into the cancer cells through endocytosis, but also need to escape from the endosomes, therefore minimizing enzymatic hydrolysis of antitumor drugs while the therapeutic effects are maximized. Endosome escape technology had been widely used in antitumor drug delivery system [25,26], the pH sensitivity induced surface protonated effect of the drug delivery system is very common mean for endosome escape [27,28], but the NIR light induced endosome escape system was rare. A MoS₂ based drug delivery system was de-

veloped, and its NIR induced endosome escape was realized in this study.

In this work, a polyethylene glycol (PEG2000) modified MoS₂ (MoS₂-PEG) with high aqueous solubility, neutral pH and accessibility to further modification, was synthesized, characterized and explored its applications in drug delivery, PTT, X-ray diagnosis and endosome escape induced by NIR. Doxorubicin (DOX), one of the most effective drugs against a wide range of cancers, was employed as the model drug and loaded onto MoS₂-PEG with high efficacy. Herein, taking advantages of the endosome escape property, potential in PTT, drug delivery and X-ray imaging ability of MoS₂-PEG, a multi-functional drug delivery system (MoS₂-PEG/DOX) (Fig. 1) was developed and characterized by transmission electron microscopy (TEM), dynamic laser scattering (DLS), Fourier transmission infrared spectroscopy (FTIR). NIR induced endosome escape, PTT, tumor-targeting and photothermal-chemo therapeutic efficacy of MoS₂-PEG/DOX was evaluated using MCF-7 cells and tumor-bearing mice models, furthermore, *in vivo* X-ray imaging of tumor-bearing mice using MoS₂-PEG is also conducted.

2. Materials and methods

2.1. Materials

Molybdenum disulfide (MoS₂, purity > 95%) were purchased from DK nano Co. Ltd Beijing. Doxorubicin (DOX, 20120503, purity > 98%) was gotten from Beijing Yi-He Biotech Co. Ltd. Thioglycolic acid (HSCH₂COOH, 70% in water), NH₂-PEG2000-OCH₃, N-(3-dimethylamino propyl)-N'-ethylcarbodiimide hydrochloride (EDC-HCl), IR 783 dye and dimethyl sulfoxide (DMSO) were obtained from Sigma-Aldrich Co. LLC. Sulforhodamine B (SRB), RPMI 1640 cell culture medium, penicillin, streptomycin, fetal bovine serum (FBS), and heparin sodium were bought from Gibco Invitrogen.

2.2. Synthesis of MoS₂-PEG/DOX

Synthesis of MoS₂ nanosheets. Two-dimensional MoS₂ nanosheets were prepared by the chemical exfoliation method according to the literature [24] (Fig. 2). In brief, 50 mg MoS₂ and 2 g NaCl were mixed and grinded for 4 h, and then NaCl was removed by repeating adding water and centrifugation. The treated MoS₂ (50 mg) was added to 20 ml of oleum, after stirring at 90 °C for 12 h, the result product (MoS₂ nanosheets) was washed by centrifugation for several times with deionized (D.I.) water, and dried in vacuum for 12 h.

Synthesis of MoS₂-COOH. The MoS₂ nanosheets (50 mg) was added to 20 ml of mercapto acid, after stirring at room temperature under protection of Ar for 24 h, the result product (MoS₂-COOH) was washed by centrifugation for several times with deionized (D.I.) water, and dried in vacuum for 12 h.

Conjugation of PEG to MoS₂-COOH. MoS₂-COOH (50 mg) was suspended with NH₂-PEG2000-OCH₃ (200 mg) in a pH 7.4 phosphate buffered saline (PBS) solution (50 ml), EDC-HCl (80 mg), and then NHS (35 mg) was added. The mixture was allowed to react at room temperature for 48 h, after which the conjugate was precipitated using 200 ml of anhydrous ethanol, then the precipitate was purified by repeated rinsing with ethanol

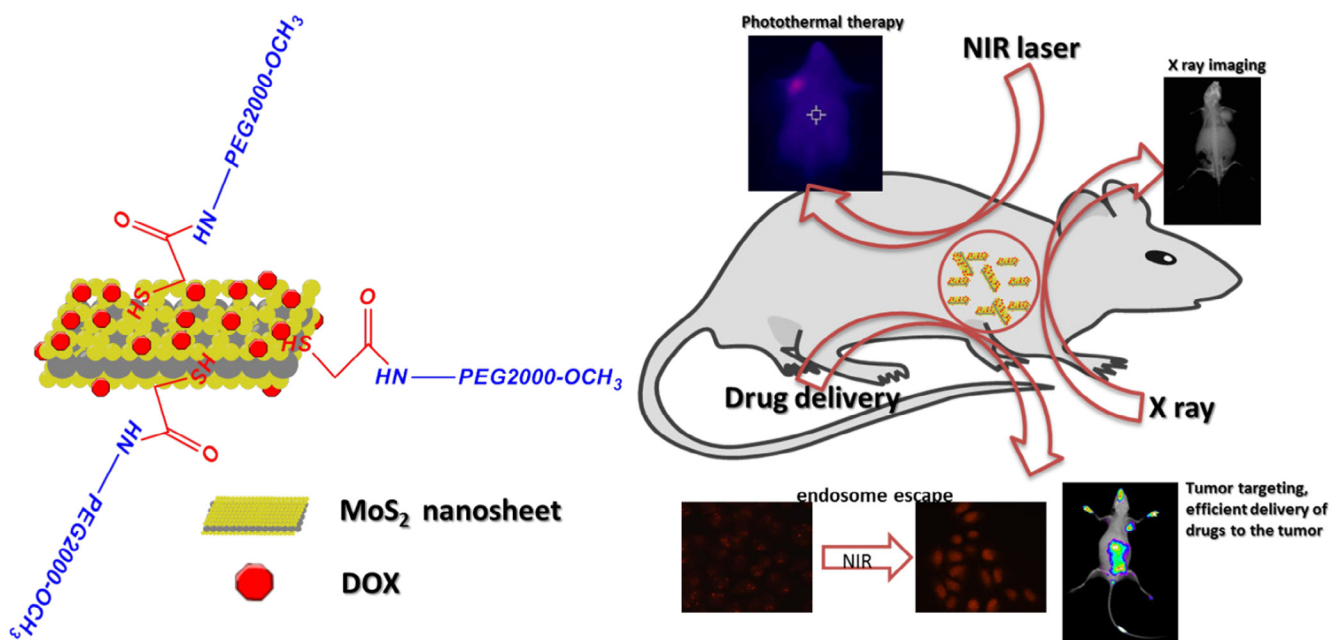


Fig. 1 – Scheme of MoS₂-PEG/DOX and its biofunctions.

and filtrations to remove the unreacted reagents to obtain MoS₂-PEG. The resulting solid products were dried in vacuum at 60 °C for 24 h.

DOX loading. MoS₂-PEG (50 mg) was added to DOX water solution (20 ml) containing DOX (150 mg) and sonicated at room temperature for 2 h and then sonicated using an ultrasonic cell disruption system (400W, 10 times), finally the nanosuspension was centrifuged to remove free DOX. The entire process was carried out in the dark, and the resulting MoS₂-PEG/DOX nanosuspension was stored at 4 °C in the dark until use. The amount of DOX loaded onto MoS₂-PEG was measured at 490 nm by UV-VIS spectrometer.

2.3. Characterization

DLS (Zetasizer Nano ZS-90, Malvern, UK) and TEM (Tecnai G2 20, FEI) were used for characterizing zeta potential and morphological of MoS₂-PEG/DOX, respectively. The optical properties of MoS₂-PEG/DOX were characterized using a UV-VIS spectrometer (Lambda 35, Perkin-Elmer, USA). FT-IR spectra were recorded on a Nicolet iS10 spectrometer (Thermo). The photothermal efficacy of MoS₂-PEG/DOX was performed using a thermal infrared imager (T200, Fluke). The *in vivo* fluorescence and X-ray images were conducted on a small animal *in vivo* imaging system (Bruke).

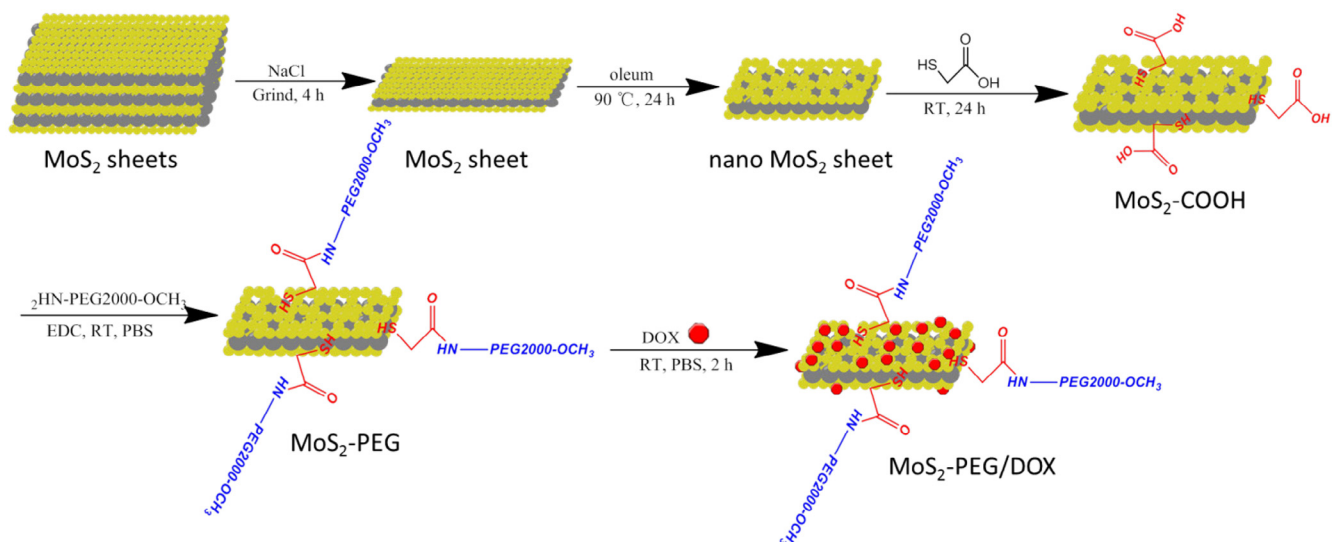


Fig. 2 – A schematic illustration of MoS₂-PEG/DOX nanocomposite preparation.

2.4. NIR induced thermal effect of MoS₂-PEG

For photothermal therapy, a NIR laser (808 nm, 1 or 2 W/cm²) was used. MoS₂-PEG in water (0.2 ml) at 10 µg/ml was illuminated with an 808 nm, continuous-wave NIR with the power density of 1 W/cm² or 2 W/cm². The temperature was measured by a thermal infrared imager (T200, Fluke).

2.5. DOX release from MoS₂-PEG/DOX

MoS₂-PEG/DOX (1 ml) was sealed in dialysis membranes (MW cutoff 1000, Spectrapor). The dialysis bags were incubated in 10 ml PBS buffer at 37 °C with a stirring rate of 100 r/min. A 200 µl portion of the aliquot was collected from the incubation medium at predetermined time intervals, and the released DOX was quantified by UV-vis spectrophotometer at 490 nm. The DOX release studies were performed in triplicate for each sample.

2.6. Cellular experiments

Cell culture. MCF-7 human breast cancer cell line was obtained from Chinese Academy of Sciences Cell Bank (Catalog No. Hyc3204). Cells were cultured in normal DMEM culture medium with 10% fetal bovine serum (FBS) and 1% penicillin/streptomycin in 5% CO₂ and 95% air at 37 °C in a humidified incubator.

Cellular uptake. Intracellular uptake of DOX and MoS₂-PEG/DOX were performed with MCF-7 cells. MCF-7 cells were seeded at 5 × 10⁴ cells/well on glass cover slips in 6-well plates. When cells reached 70% confluence, they were treated with DOX (10 µg/ml) and MoS₂-PEG/DOX (DOX concentration: 10 µg/ml and MoS₂-PEG concentration: 14.5 µg/ml) for 0.5, 2 and 6 h, respectively. After washing three times with PBS, the cells were imaged by a Fluorescence Microscope (Zeiss LSM 510).

NIR induced endosome escape. MCF-7 cells were seeded at 5 × 10⁴ cells/well on glass cover slips in 6-well plates. When cells reached 70% confluence, they were treated with MoS₂-PEG/DOX (DOX concentration: 10 µg/ml and MoS₂-PEG concentration: 14.5 µg/ml) for 2 h, after incubation, cells were washed twice with PBS, and then a NIR laser (808 nm, 2 W/cm², 5 min) was delivered to culture dish. After irradiation, the DOX signal in MCF-7 cells were acquired using a Fluorescence Microscope (Zeiss LSM 510).

In vitro PTT. To investigate the PTT effect of MoS₂-PEG on cancer cells, the MCF-7 cells were cultured and lifted as described above before seeding (1 × 10⁴) into 96-well plates and incubating for 24 h. The medium then was replaced with fresh medium containing various concentrations of free MoS₂-PEG for 6 h, the cells were or were not irradiated with a NIR laser (808 nm, 2 W/cm²) for 5 min. At last a standard cell viability assay using SRB was conducted. MCF-7 cells were seeded into a 6-well plates, after incubating with MoS₂-PEG (10 µg/mL) for 6 h, PI was loaded into the cells. After 30 min incubation, a NIR laser (2 W/cm²) was delivered to the center of the plate for 5 min. At last, fluorescence images in red field were acquired using a Fluorescence Microscope (Zeiss LSM 510).

In vitro photothermal-chemotherapy. To investigate combination therapeutic effect of PTT and chemotherapy of MoS₂-PEG/DOX, MCF-7 cells were seeded at 1 × 10⁴ cells/well on glass

cover slips in 96-well plates for 24 h. The medium then was replaced with fresh medium containing free DOX and MoS₂-PEG/DOX (the same DOX concentration) for 6 h, the cells were or were not irradiated with a NIR laser (808 nm, 2 W/cm²) for 5 min. At last a standard cell viability assay using SRB was conducted.

Cells apoptosis assay. Apoptosis was monitored by an Annexin-V-Fluos Staining kit (Sigma-Aldrich Co. LLC). MCF-7 cells were treated with free DOX (5 µg/ml), MoS₂-PEG (7.3 µg/ml) and MoS₂-PEG/DOX (DOX concentration: 5 µg/ml, MoS₂-PEG concentration: 7.3 µg/ml) for 6 h, the cells were or were not irradiated with a NIR laser (808 nm, 2 W/cm²) for 5 min, then trypsinized, washed with PBS, and re-suspended in binding buffer (10 µM HEPES/NaOH, pH 7.4, 140 µM NaCl, and 2.5 µM CaCl₂). After adjusting cell density to 1 × 10⁶ cell/ml, 1 µl of recombinant human anti-Annexin V-FITC and 2 µl of propidium iodide (PI) were added to 100 µl of cell suspension, mixed by a vortex and incubated at room temperature in the dark for 15 min. Finally, 400 µl binding buffer was added to the above cells and subsequently analyzed by Flow Cytometry (FCM, Epics XL.MCL).

2.7. In vivo experiments

Xenograft tumor mouse model. All animal experiments were performed under a protocol approved by Henan laboratory animal center. The S180 tumor models were generated by subcutaneous injection of 2 × 10⁶ cells in 0.1 ml saline into the right shoulder of female BALB/c mice (18–20 g, Henan laboratory animal center). The mice were treated when the tumor volume reached 60 to 100 mm³ (~6 days after tumor inoculation).

Toxicity test of MoS₂-PEG. For the acute toxicity, 120 mg/kg, 60 mg/kg and 10 mg/kg of MoS₂-PEG (all in 0.2 ml solution) were intravenously injected into tumor-bearing mice (6 mice per group). For the long-term toxicity, 20 mg/kg of MoS₂-PEG were intravenous injected into tumor-bearing mice (6 mice per group) every 2 d for 14 d, the number of hemocytes and the transaminase in blood were determined after 14 d treatment.

In vivo biodistribution of MoS₂-PEG. A near-infrared dye (IR783) was used to mark MoS₂-PEG: IR783(50 µg) was added to MoS₂-PEG nanosuspension (1 mg/ml, 5 ml) and ultrasonicated with ultrasonic cell disruption system to obtain MoS₂-PEG/IR783. Excess IR783 was removed by Sephadex G-25 column (Sigma Aldrich Co. LLC). 0.2 ml of MoS₂-PEG/IR783 were intravenously injected into tumor-bearing mice, and the whole body fluorescence imaging were performed at 1 min, 30 min, 4 h, 8 h and 24 h after injection.

Biodistribution of DOX. 0.2 ml of DOX (5 mg/kg) and MoS₂-PEG/DOX (DOX: 5 mg/kg, MoS₂-PEG: 7.3 mg/kg) were intravenously injected into tumor-bearing mice (6 mice per group). After injection for 0.5, 4, 8 and 12 h, the mice were killed to collect heart, liver, spleen, lung, kidney and tumor, weighed, and homogenized in buffer (methanol to saline ratio, 1:1). DOX in tumors were determined by high performance liquid chromatography (HPLC, 1100 Agilent, USA) under the following chromatographic conditions: an Eclipse XDB-C18 column (150 mm × 4.6 mm, 5.0 µm); mobile phase sodium acetate solution (0.02 mol/L)/acetonitrile 80:20; column temperature 40 °C; fluorescence detector with the excitation and emission

wavelengths set at 475 nm and 525 nm, respectively; flow rate 1.0 mL/min; and injection volume 20 μ L.

In vivo antitumor effect. For the *in vivo* antitumor experiments, the tumor-bearing mice were divided into seven groups (six mice per group), minimizing the differences of weights and tumor sizes in each group. The mice were administered with (1) saline (0.2 ml), (2) saline/NIR (0.2 ml), (3) MoS₂-PEG (7.3 mg/kg), (4) DOX (5 mg/kg), (5) MoS₂-PEG/DOX (DOX: 5 mg/kg, MoS₂-PEG: 7.3 mg/kg), (6) MoS₂-PEG/NIR (7.3 mg/kg, 808 nm laser, 2 W/cm², 5 min) and (7) MoS₂-PEG/DOX/NIR (DOX: 5 mg/kg, MoS₂-PEG: 7.3 mg/kg, 808 nm laser, 2 W/cm², 5 min) were intravenously injected into mice via tail vein every 2 days, respectively, the irradiating groups were exposed to 808 nm laser at 8 h post-injection. The mice were observed daily for clinical symptoms and the tumor sizes were measured by a caliper every other day and calculated as the volume = (tumor length) \times (tumor width)²/2. After treatment for 14 days, the mice were killed to collect tumor tissue for H&E staining. Morphological changes were observed under microscope (Zeiss LSM 510).

In vivo X-ray imaging. For *in vivo* X-ray imaging, the tumor-bearing mice were intravenously injected with MoS₂-PEG/DOX (DOX: 10 mg/kg, MoS₂-PEG: 14.5 mg/kg), after injection for 0.5, 4, 8 and 12 h, X-ray imaging was conducted on a small animal *in vivo* imaging system (Bruke). Iohexol (a clinical X-ray contrast agent, 240 mg/ml, 0.1 ml) and MoS₂-PEG (8 mg/ml, 0.1 ml) were subcutaneously injected into a health mice, and the X-ray imaging effect was also tested by the small animal *in vivo* imaging system (Bruke).

2.8. Statistical analysis

Quantitative data are expressed as mean \pm SD and analyzed by use of Student's *t* test. *P* values < 0.05 were considered statistically significant.

3. Results and discussions

3.1. Synthesis and characterization of MoS₂-PEG/DOX

The large and multi-layered structure of MoS₂ greatly limits its applications in drug delivery [29], therefore, in this study, two-dimensional MoS₂ nanosheets were prepared by the chemical exfoliation method according to the literature (Fig. 2). Although MoS₂ nanosheets produced by this method increased its water solubility via reducing the size and the number of layers, they were only stable in water within 1 h at the room temperature (Fig. 3F). In order to further increase its water solubility, PEGylation was performed in this study. More Mo atoms were exposed on the surface of MoS₂ nanosheets after the oleum treatment, and according to the metallic character of Mo atoms in MoS₂ nanosheets, sulfhydryl substances were easily conjugated to the Mo, we firstly modified the MoS₂ nanosheets with thioglycolic acid (Fig. 2). The successful conjugation of thioglycolic acid to the MoS₂ nanosheets (MoS₂-COOH) was confirmed by FT-IR spectrum (Fig. 3A), compared with the MoS₂ nanosheets, MoS₂-COOH gave a strong C = O (\sim 1710 cm⁻¹) vibrations, indicating -COOH was introduced to MoS₂ nanosheets. PEGylation was performed to improve the solubility and

biocompatibility of MoS₂ nanosheets, NH₂-PEG2000-OCH₃ were reacted with amino to form amide bonds and linked to the MoS₂-COOH via carboxyl bonds (Fig. 2), the successful of PEGylation was also proved by FT-IR (Fig. 3A), compared with MoS₂-COOH, MoS₂-PEG gave the extra peaks at amide I (\sim 1662 cm⁻¹) vibrations, amide III (\sim 1388 cm⁻¹) vibrations and C-H (\sim 1127 cm⁻¹) vibrations, and MoS₂-PEG exhibited excellent stability in water (Fig. 3F).

In this work, DOX, one of the most effective drugs against a wide range of cancers, was loaded onto MoS₂-PEG through a physical adsorption. DOX loaded onto MoS₂-PEG was confirmed by a strong absorption peak at around 495 nm over the background of MoS₂-PEG in UV-VIS spectrum (Fig. 3E). MoS₂-PEG/DOX was stable in water, PBS buffer, cell culture medium and plasma of mice over multiple weeks without significant aggregation (Fig. 3F). The amount of DOX loaded onto MoS₂-PEG was calculated to be 69 wt%.

The morphology of MoS₂ and MoS₂-PEG/DOX nanosystem were characterized by TEM. As can be seen from TEM image (Fig. 3B and C), MoS₂ had a large and multi-layered structure, while MoS₂-PEG/DOX nanosheet was much smaller and obviously decreased the number of the layers, indicating that the chemical exfoliation and PEGylation were successful. MoS₂-PEG/DOX showed a 2D structure with the size of 150 nm. The zeta potential of MoS₂-PEG/DOX was -7.17 ± 1.8 mV, and zeta potential distribution were shown in Fig. 3D.

3.2. Increased temperature under NIR irradiation

After NIR irradiation for 5 min, the temperature of MoS₂-PEG (10 μ g/ml, 1 W/cm² or 2 W/cm²) samples increased 11.1 and 17.8 $^{\circ}$ C, respectively, while water increased 1.9 $^{\circ}$ C (Fig. 4). The temperature increase of MoS₂-PEG showed NIR power density and NIR radiation time-dependent manners (Fig. 4), revealing that MoS₂-PEG was an effective photothermal agent in cancer therapy.

3.3. DOX release from MoS₂-PEG/DOX

Herein, the release behavior of DOX from MoS₂-PEG/DOX was shown in Fig. 5, showing a sustain release over 48 h. In contrast, DOX release in DOX group was considerably fast, and almost 91.3% of the drug released after 12 h, indicating that interaction between MoS₂-PEG and DOX plays a critical role in the release of drug.

3.4. X-ray imaging

MoS₂ have a great potential as a contrast agent in X-ray imaging, in order to investigate the X-ray imaging ability of MoS₂-PEG, MoS₂-PEG in water with different concentrations were conducted on a small animal *in vivo* imaging system (Bruke), and the result was shown in Fig. 6. In order to further examine the X-ray imaging ability of MoS₂-PEG, iohexol, a clinical X-ray contrast agent with a clinical dosage (240 mg/ml) was used in this study as a positive control, the X-ray images of MoS₂-PEG (8 mg/ml) and iohexol (240 mg/ml) were also shown in Fig. 6. Compared with iohexol, MoS₂-PEG exhibited stronger X-ray signal, suggesting that MoS₂-PEG had a stronger X-ray imaging ability than iohexol, and the X-ray signal of MoS₂-PEG was

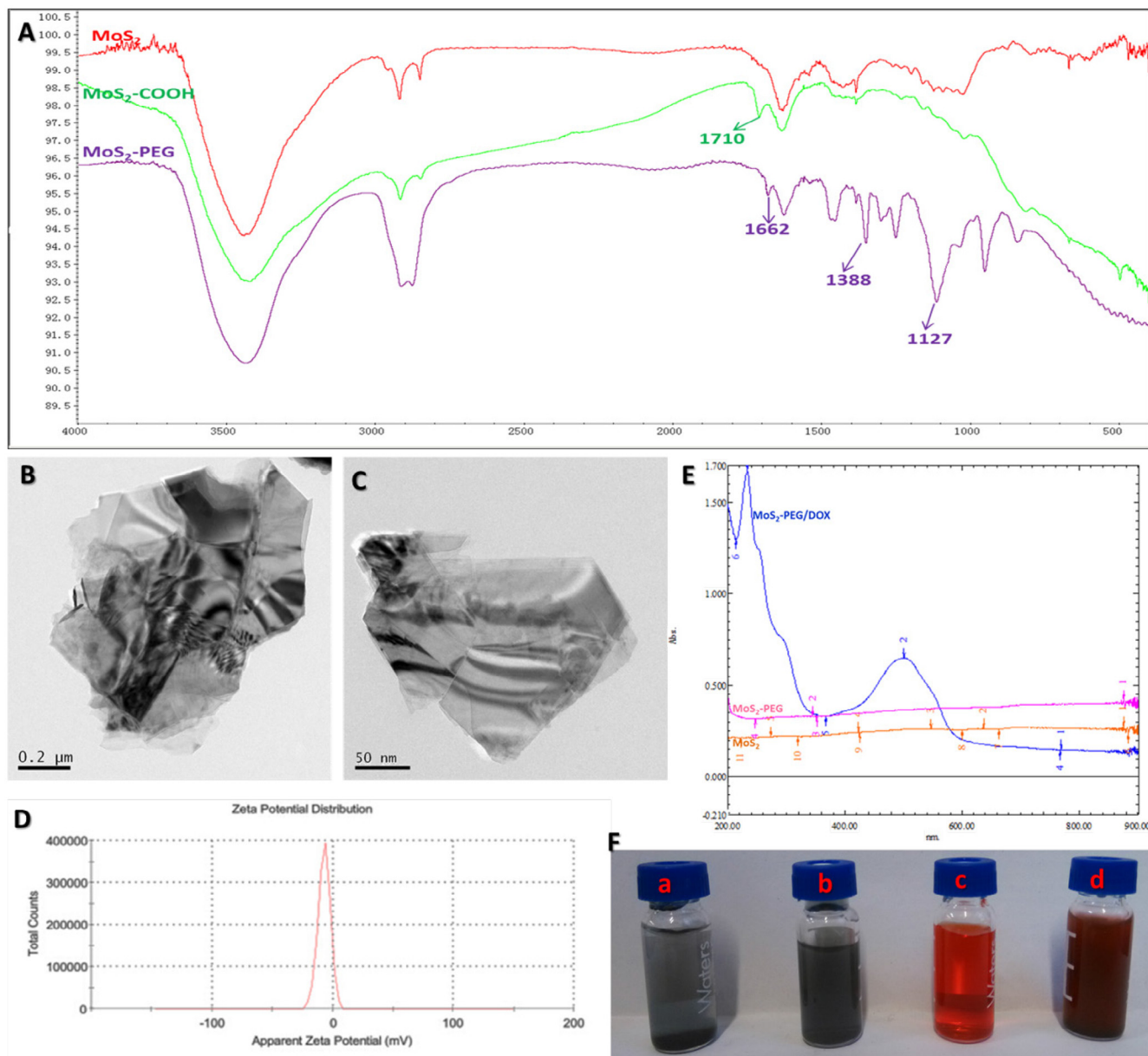


Fig. 3 – Characterization of MoS₂-PEG/DOX. A) FT-IR spectrum of MoS₂, MoS₂-COOH and MoS₂-PEG; **B)** and **C)** TEM images of MoS₂ and MoS₂-PEG/DOX; **D)** Zeta potential distribution of MoS₂-PEG/DOX; **E)** UV-VIS spectrum of MoS₂, MoS₂-PEG and MoS₂-PEG/DOX; **F)** MoS₂ (a), MoS₂-PEG (b), DOX (c) and MoS₂-PEG/DOX (d) in water.

increasing with the concentration increased, revealing a concentration-dependent manner.

3.5. Cellular uptake

To explore the uptake of MoS₂-PEG/DOX by MCF-7 cells, we tracked DOX internalization into the cells through colocalization of DOX-signal (red fluorescence). As can be seen from Fig. S3, cells incubated with MoS₂-PEG/DOX for different time clearly revealed the time-dependent cellular uptake manner. Cells exposed to free DOX showed a stronger fluorescence intensity of DOX in the nucleus after 2 h of incubation, while in the

case of MoS₂-PEG/DOX, red fluorescence was observed mainly in the endosomes (Fig. S3), indicating that MoS₂-PEG/DOX were initially located within the endosomal intracellular compartments. After 6 h of incubation, the cells exposed to MoS₂-PEG/DOX demonstrated an obvious increase of red fluorescence in the cell nucleus, suggesting that with the passage of time, on one hand, MoS₂-PEG/DOX arrived at the cell cytoplasm from the endosomes gradually, on the other hand, DOX was released from MoS₂-PEG/DOX to cytoplasm, then the intracellular DOX in the cytosol were rapidly transported to the nucleus and avidly bound to the chromosomal DNA [44]. This distinction in uptake could explain the difference in susceptibility of MoS₂-PEG/DOX and DOX to MCF-7 cells.

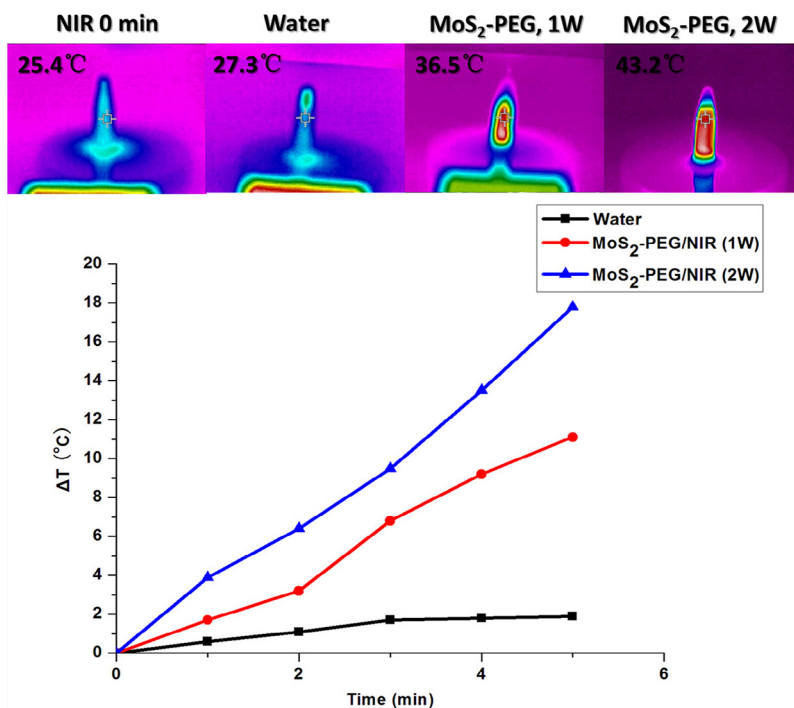


Fig. 4 – Temperature evolution of MoS₂-PEG during continuous radiation by NIR at a power density of 1 W/cm² or 2 W/cm².

3.6. In vitro PTT

Cytotoxicity of MoS₂-PEG is an important consideration for materials intended for *in vivo* application. Toward this goal, assessment of cell viability of MCF-7 cancer cells was examined. Incubation with MoS₂-PEG showed that there were minimal decrease in cell viability (<15%), even when the cells were incubated with 100 μg/mL of MoS₂-PEG for 24 h (Fig. S4), demonstrating that MoS₂-PEG possess low toxicity without NIR

laser irradiation. In order to further investigate the toxicity of MoS₂-PEG with high concentration, the level of intracellular reactive oxygen species (ROS) was also determined in this study, from Fig. S1, we can see that 100 μg/mL of MoS₂-PEG did not significantly increase the intracellular ROS, and MoS₂-PEG could not significantly induce the oxidative stress of MCF-7 cells, suggesting MoS₂-PEG had little cytotoxicity to MCF-7 cells.

PTT usually employs hyperthermia agents to induce photothermal damage of tumor cells under NIR light [30]. Owing

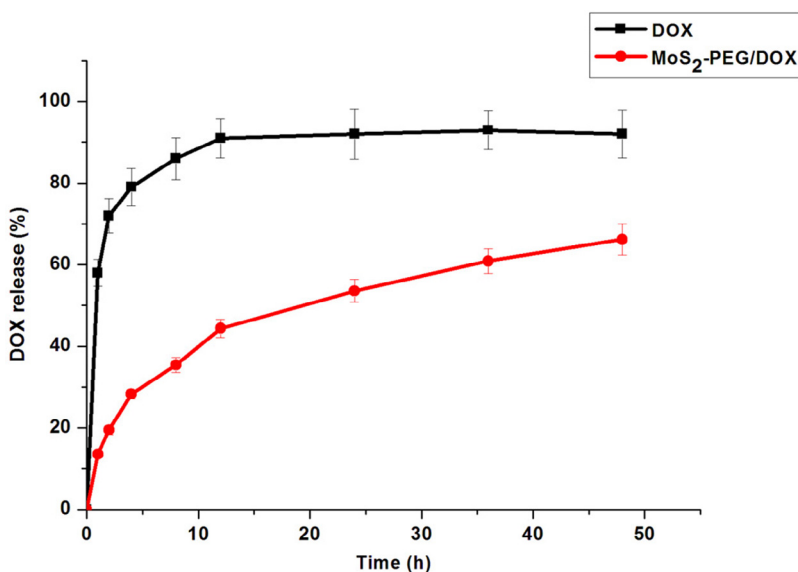


Fig. 5 – Release profiles of DOX from MoS₂-PEG/DOX and DOX solution. Data were presented as mean ± standard deviation (n = 3).

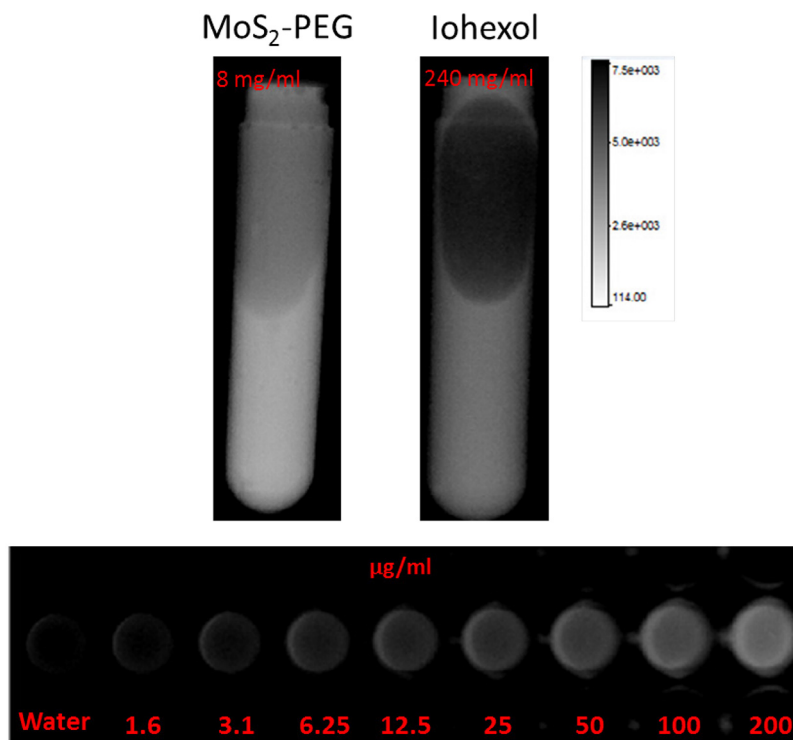


Fig. 6 – X-ray images of iohexol and MoS₂-PEG in water with different concentrations.

to its strong absorption in NIR window, MoS₂-PEG was utilized for photothermal ablation of cancer cells under NIR in this study. MCF-7 cells were incubated with MoS₂-PEG at different concentrations for 6 h and then exposed to a 808 nm NIR laser at a power density of 1 W/cm² or 2 W/cm² for 5 min. Fig. 7A showed that the viabilities of untreated cells were not noticeably affected under NIR laser (>97%), however, MoS₂-PEG incubated MCF-7 cells were largely killed after NIR

irradiation, showing decreasing cell viabilities as the concentration of MoS₂-PEG increased. Besides, the cell viabilities of MoS₂-PEG/NIR (2 W/cm²) was much lower than that of 1 W/cm², revealing that the PTT efficacy of MoS₂-PEG showed a concentration-dependent manner, and a NIR power density-dependent manner. Fig. 7B showed that a large amount of cancer cells were killed in the NIR laser region, while the dead cells outside the NIR laser region were less, indicating that NIR

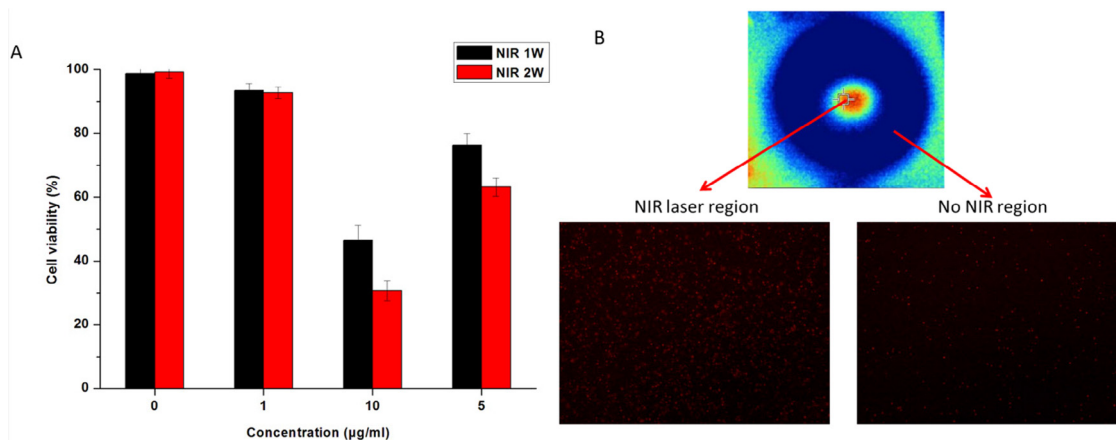


Fig. 7 – (A) NIR thermal ablation of MCF-7 cells (NIR: 808 nm laser, 5 min). (B) Fluorescence images of PI (red, dead cells) stained cells treated with MoS₂-PEG (10 µg/ml) for 6 h in NIR region (NIR: 808 nm laser, 2 W/cm², 5 min) and No NIR region, the NIR region and No NIR region were in one cell culture dish. Data were presented as mean ± standard deviation (n = 6).

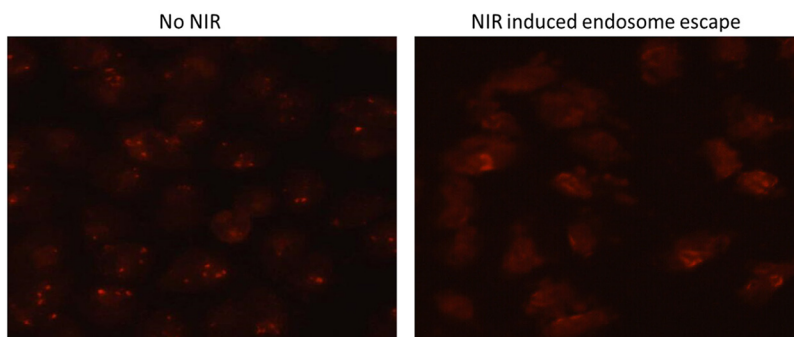


Fig. 8 – Fluorescence images of MCF-7 cells incubated MoS₂-PEG/DOX for 2 h with or without NIR laser radiation (NIR: 808 nm laser, 2 W/cm², 5 min) (200×).

laser based PTT had a good positioning property, and this advantage make PTT have a great potential application in the *in vivo* tumor therapy.

3.7. NIR induced endosome escape

MoS₂-PEG/DOX nanosheets entered the MCF-7 cells via endocytosis, when the cells were treated with MoS₂-PEG/DOX (DOX concentration: 10 µg/ml, MoS₂-PEG concentration: 14.5 µg/ml) for 2 h, the red fluorescence (DOX signal) was concentrated in the cells, indicating MoS₂-PEG/DOX was mainly in the endosomes (Fig. 8), while after 5 min of NIR radiation (808 nm laser, 2 W/cm²), the DOX signal obviously spread to the entire cell (Fig. 8). In order to exclude the influence of DOX release from MoS₂-PEG/DOX under NIR laser, a DOX release experiment under NIR laser was performed, and the result showed that the DOX release did not have significant change combined with NIR laser irradiation. Therefore, we inferred that MoS₂-PEG/DOX could escape from endosome under NIR irradiation, and MoS₂-PEG/DOX spread to the entire cell quickly. NIR induced endosome escape needs two conditions, the first one is MoS₂-PEG/DOX must be close to the membrane of endosome, and we found that compared with PEG, MoS₂ had a stronger adsorption capacity on phospholipid, this property of MoS₂ make MoS₂ based system have the ability of cling to even insert to the endosome membranes. The other condition is MoS₂-PEG/DOX must generate a large amount of heat under NIR laser, and this was already proved in section 3.2. In summary, MoS₂-PEG/DOX clung to the membrane of endosome, when the NIR radiation came, MoS₂-PEG/DOX generated a large amount of heat, and the heat induced the rupture of the membrane, at last MoS₂-PEG/DOX could escape from endosome. NIR induced endosome escape of MoS₂-PEG/DOX reduced the loss and improved the therapeutic efficacy of DOX.

3.8. Photothermal-chemotherapy *in vitro*

Recently, combination therapy is more and more popular in cancer therapy, for examples, photothermal-chemotherapy [31], photodynamic-chemotherapy [32], and combination therapy always displays higher efficiency than any single treatment, therefore MoS₂-PEG/DOX was utilized for cancer photothermal-chemotherapy in this study. MCF-7 cells were incubated with DOX and MoS₂-PEG/DOX at different concentrations for 6 h and

then exposed to NIR at a power density of 2 W/cm² for 5 min. The combination therapeutic efficiency was shown in Fig. 9. There was no significant difference in cell viability between DOX-treated and MoS₂-PEG/DOX-treated cells. Compared with no NIR groups or DOX alone group, the NIR radiation greatly enhanced the cytotoxicity of MoS₂-PEG/DOX especially in the concentration groups. The lower cell-killing ability in the low concentration groups could be attributed to insufficient MoS₂-PEG to producing enough heat to kill cells. At a DOX concentration of 5 µg/ml with MoS₂-PEG concentration of 7.3 µg/ml, the inhibition rate of MoS₂-PEG/DOX/NIR was significantly increased to around 81.3%, while MoS₂-PEG/DOX and MoS₂-PEG/NIR (10 µg/ml) were around 58.2% and 59.3% respectively, indicating an enhanced cell-killing effect, thus, a synergistic therapeutic effect of PTT induced by MoS₂-PEG and DOX was observed on MCF-7 cells. Besides PTT, NIR laser could also stimulate endosome escaping to improve the efficiency of DOX, this might be another reason for the higher therapeutic efficacy of MoS₂-PEG/DOX/NIR than MoS₂-PEG/DOX.

3.9. MCF-7 cells apoptosis

To further understand the therapeutic efficacy of combination treatment group, the cell apoptosis experiment was also investigated. DOX and MoS₂-PEG/DOX treatment significantly enhanced the cell apoptosis ($P < 0.05$), while the PTT treatment groups significantly enhanced the cell necrotic ($P < 0.05$), the number of health cells in MoS₂-PEG/DOX treatment group was around 2.2%, much less than the other groups (Fig. 10), showing the combination therapy was most effective, and the result was consistent with the cell viability studies.

3.10. Toxicity of MoS₂-PEG *in vivo*

As MoS₂ is a new material in biomedicine, its toxicity is the most important consideration for further applications. Therefore, we investigated the toxicity of MoS₂-PEG in this study. For the acute toxicity, 120 mg/kg, 60 mg/kg and 10 mg/kg of MoS₂-PEG were intravenously injected into tumor-bearing mice (6 mice per group), and the injection volume was 0.2 ml. No mouse died after injection for 5 d, even at a very high MoS₂-PEG dosage (120 mg/kg), indicating that MoS₂-PEG had a low toxicity *in vivo*. In order to further understand the injury especially the inflammation and liver damage induced by MoS₂-PEG, long term

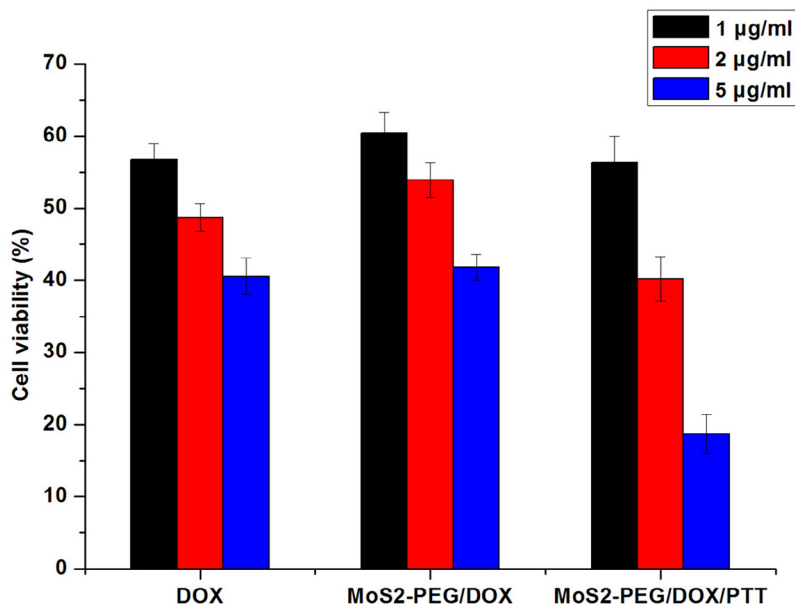


Fig. 9 – Cell viability of different treatments on MCF-7 cells. For PTT: 808 nm laser, 2 W/cm², 5 min. Data were presented as mean ± standard deviation (n = 6).

toxicity was also performed. 20 mg/kg of MoS₂-PEG were intravenously injected into tumor-bearing mice (6 mice per group) every 2 d for 14 d, no mouse died at the end, the number of hemocytes and the content of alanine aminotransferase (ALT)

in blood after 14 d treatment were shown in Fig. S5, the number of white blood cells (WBC), red blood cells (RBC) and platelets (PLT) in blood did not significantly increase, demonstrating that MoS₂-PEG did not induce the obvious inflammation *in vivo*. The

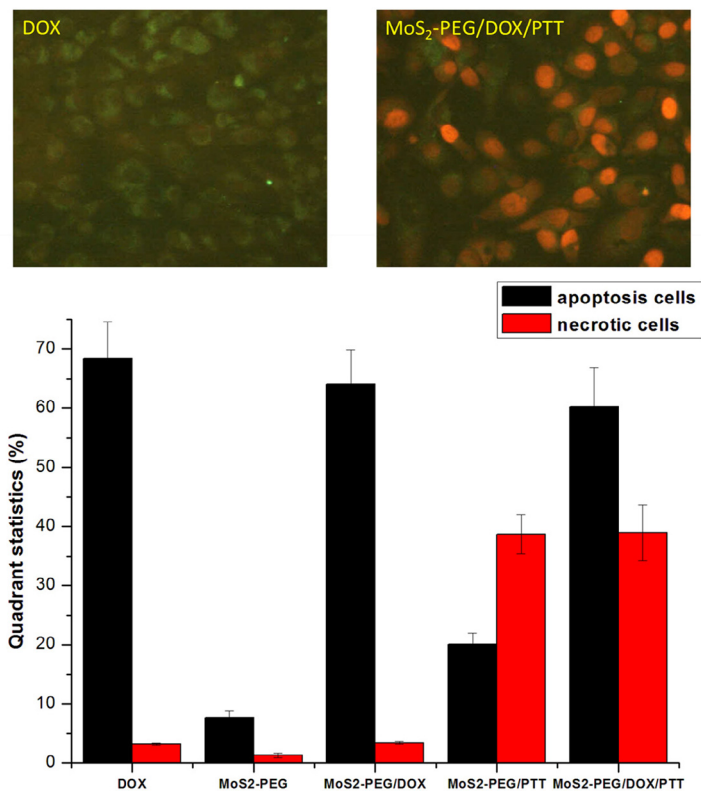


Fig. 10 – Cell apoptosis studies of different treatments on MCF-7 cells. DOX concentration: 5 µg/ml, MoS₂-PEG/DOX concentration: 7.3 µg/ml; For PTT: 808 nm laser, 2 W/cm², 5 min. Data were presented as mean ± standard deviation (n = 6) (200×).

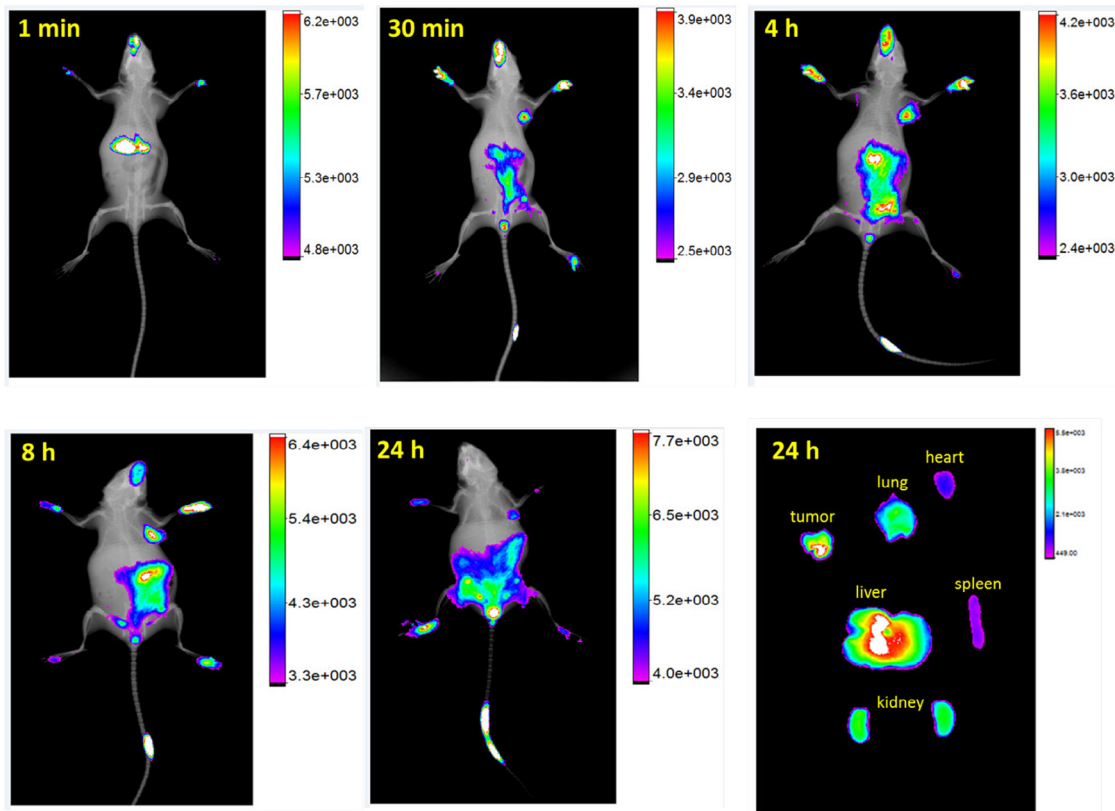


Fig. 11 – The *in vivo* biodistribution of MoS₂-PEG/IR783 for different times.

content of ALT in blood is an important indicator of liver damage, and the level of ALT directly reflects the degree of liver damage [33,34], the content of ALT after treatment was shown in Fig. S5B. Compared with the control group, the content of ALT in MoS₂-PEG-treated group increased ($P < 0.05$), but the increased amount of ALT was little, indicating that MoS₂-PEG (20 mg/kg) treatment for 14 d slightly induced the liver damage of the mice. In the following *in vivo* studies, the dosage of MoS₂-PEG we used was 7.3 mg/kg, which was much lower than 20 mg/kg, so we thought the dosage of MoS₂-PEG used in this study may not be noticeably toxic to mice.

3.11. Biodistribution studies

In order to investigate the biodistribution behavior of MoS₂-PEG, a near-infrared dye (IR783) was used to mark MoS₂-PEG. The biodistribution of IR783 alone was shown in Fig. S2. After injection of IR783 for 1 min, the fluorescence signal was mainly in liver, 30 min later, the signal was in liver and tumor, the fluorescence signal was mainly in bladder after 4 h of injection, indicating IR783 was cleared by the body after injection for 4 h.

Meanwhile, the biodistribution of MoS₂-PEG/IR783 was shown in Fig. 11, after injection for 1 min, the signal of MoS₂-PEG/IR783 was mainly in liver, 30 min later, it was in tumor site, and increased from 30 min to 8 h after injection. Compared with 8 h, the signal of MoS₂-PEG/IR783 in tumor at 24 h decreased, but still had a high level. Twenty-four hours after injection, the amount of MoS₂-PEG/IR783 in heart, liver, spleen, lung, kidney and tumor was also shown in Fig. 11, stronger fluorescence

signal was observed in tumor and liver, indicating MoS₂-PEG was mainly in tumor and liver 24 h after injection, showing that MoS₂-PEG could significantly accumulate in the tumor site via EPR effect, suggesting MoS₂-PEG had a great potential in drug delivery for tumor targeting therapy. Eight hours after injection, more signal of MoS₂-PEG/IR783 was observed in tumor than the other time points, so in the following *in vivo* tumor growth inhibition studies, the NIR laser irradiation time was set at 8 h after injection. The high distribution of MoS₂-PEG in tumor and low distribution in heart, spleen, lung and kidney give MoS₂-PEG a great advantage for antitumor drug delivery.

To understand tumor treatment efficacy of DOX and MoS₂-PEG/DOX, the biodistribution of DOX was investigated (Fig. 12). MoS₂-PEG/DOX showed noticeable DOX activity in blood at all the time points after injection, whereas DOX levels in the blood were much lower in the DOX group ($P < 0.01$), indicating that MoS₂-PEG/DOX significantly increased the blood circulation time of DOX *in vivo*. The DOX levels in tumor were sustained increasing from 30 min to 8 h after injection, and this result was consistent with the distribution of MoS₂-PEG, indicating that DOX and MoS₂-PEG was one system *in vivo*. Compared with DOX, MoS₂-PEG/DOX significantly decreased the distributions of DOX in heart, spleen and kidney, and this would greatly decrease the side effects of DOX to heart, spleen and kidney. Importantly, MoS₂-PEG/DOX afforded much higher DOX uptake in tumor than DOX ($P < 0.05$). The DOX level in tumor of MoS₂-PEG/DOX was higher than that of in DOX group by 5.4-fold at 8 h after injection and by 11.6-fold higher at 12 h after injection (Fig. 12). The ability of higher drug delivery efficiency to

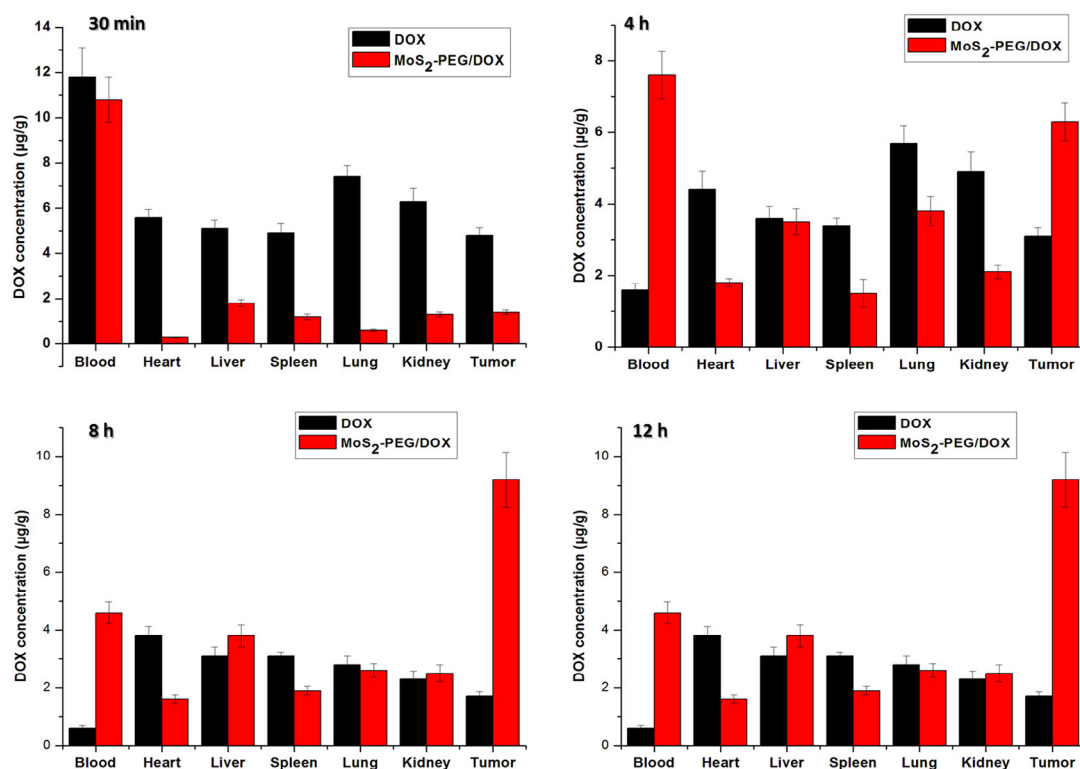


Fig. 12 – Distributions of DOX and MoS₂-PEG/DOX in tumor bearing mice. Data were presented as mean ± standard deviation ($n = 3$).

tumor by MoS₂-PEG/DOX was striking and directly responsible for the higher tumor suppression efficacy than DOX.

3.12. Tumor growth inhibition in vivo

To investigate *in vivo* treatment efficacy of MoS₂-PEG/DOX, comparative efficacy studies were conducted. The S180 tumor-bearing mice were divided into 7 groups and were treated according to protocols as summarized in method section 2.7. The changes of relative tumor volume as a function of time were plotted in Fig. 13A. The mice treated with NIR laser alone and MoS₂-PEG without NIR laser irradiation did not show any therapeutic effect, suggesting that NIR laser and the blank carrier would not affect the tumor growth. Compared with MoS₂-PEG (5.1 ± 0.44), the MoS₂-PEG/NIR resulted in V/V_0 of 3.4 ± 0.33 , in order to further understand the therapeutic efficiency of PTT, a thermal effect of PTT in tumor site were investigate (Fig. 13B). Compared with before NIR irradiation, the tumor site irradiated for 5 min showed an obvious increase of temperature (~ 10.7 °C). DOX had a relative tumor volume (V/V_0) of 2.7 ± 0.26 , while MoS₂-PEG/DOX resulted in V/V_0 of 1.3 ± 0.29 , suggesting that MoS₂-PEG/DOX could bring more DOX into the tumor site. MoS₂-PEG/DOX/NIR had a V/V_0 of 0.66 ± 0.21 , and it is significantly more effective than the other therapeutic groups ($P < 0.05$). Remarkably synergistic enhanced therapeutic effect was observed in the combination treatment group.

The therapeutic efficacy was also evaluated by H&E staining (Fig. 13C). Compared with the control group, a large amount of cell death in tumor tissue was observed in the mice treated

with MoS₂-PEG/DOX/NIR. The above results of H&E staining were consistent with the *in vivo* antitumor effect.

Allowing for high toxicity usually leads to weight loss, the body weight of all the groups were investigated. As can be seen from Fig. 13D, free DOX resulted in a significant decrease (2.00 ± 0.21) in body weight over the experimental period, while the other groups overall gained in body weight. These results indicated that MoS₂-PEG/DOX increased the therapeutic index of DOX. Furthermore, MoS₂-PEG/DOX can expectedly accumulate in tumor by escaping through the abnormally leaky tumor blood vessels and reduce the distribution in the normal organs [35,36], and this could effectively reduce the side effects of DOX during the treatment.

3.13. In vivo X-ray imaging

MoS₂ had shown a great potential as the contrast agent for X-ray imaging, so in this study, MoS₂-PEG/DOX was also used as a contrast agent for X-ray imaging. After injection of MoS₂-PEG/DOX (DOX: 10 mg/kg, MoS₂-PEG: 14.5 mg/kg) for 0.5, 4, 8 and 12 h, the X-ray images were shown in Fig. 14. Compared with control, the X-ray signals of MoS₂-PEG/DOX in tumor were significantly increased after injection of MoS₂-PEG/DOX for 0.5, 4 and 8 h, while the X-ray signal decreased at 12 h. The X-ray signals of MoS₂-PEG/DOX were obviously observed in tumor after injection for 8 h, indicating that MoS₂-PEG could accumulate in tumor, and have a great potential in tumor X-ray diagnostic applications. In order to further examine the X-ray imaging ability of MoS₂-PEG *in vivo*, MoS₂-PEG (8 mg/ml) and iohexol, a clinical X-ray

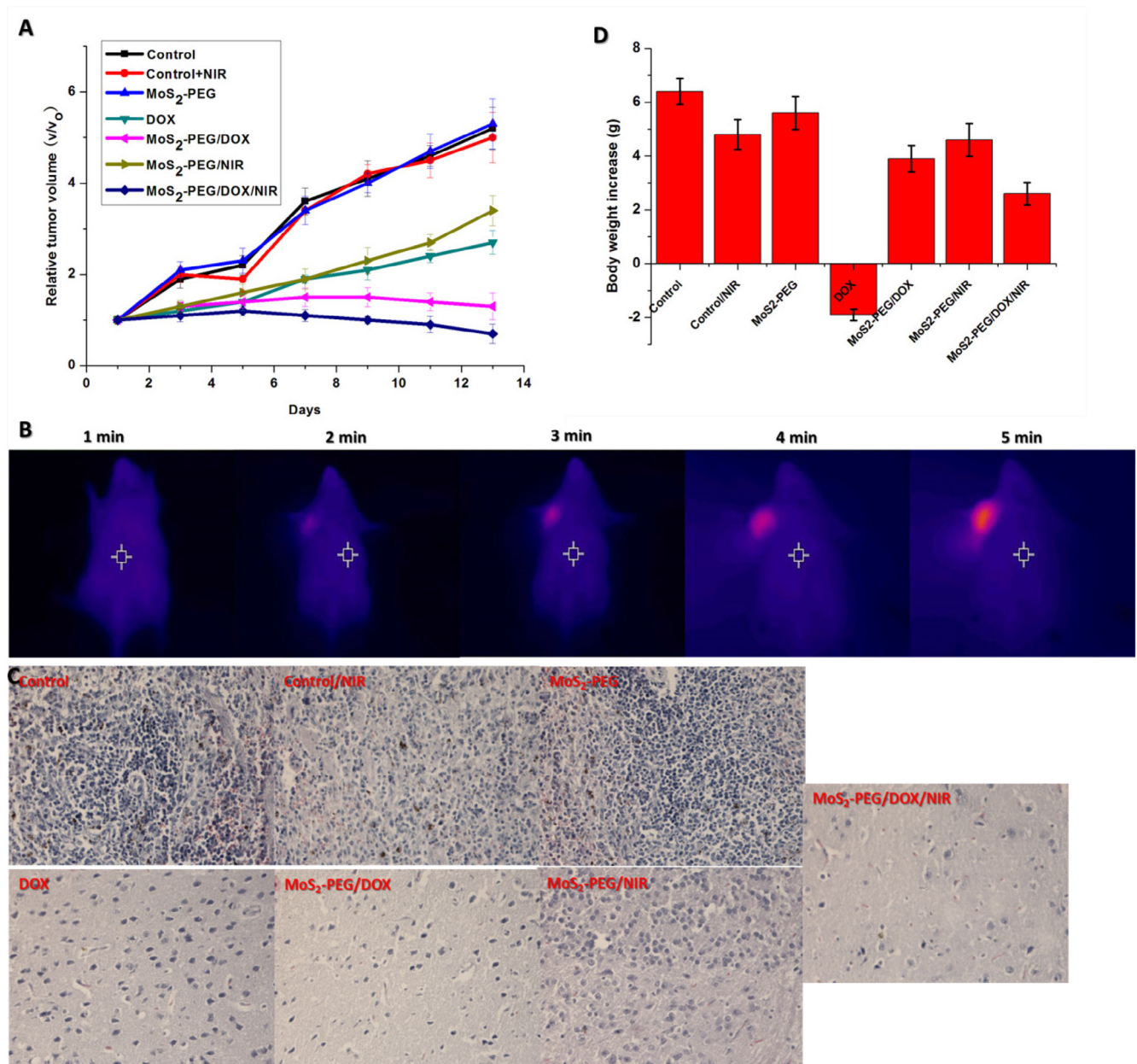


Fig. 13 – In vivo treatments (A) Tumor growth of mice in different treatment groups within 14 days; (B) Increased temperature in tumor under NIR radiation (808 nm, 2 W/cm²); (C) H&E stained tumor tissues harvested from the mice with different treatments (40×) and (D) Changes of body weight of mice in different groups during treatment. Data were presented as mean ± standard deviation (n = 6).

contrast agent with a clinical dosage (240 mg/ml) were subcutaneously injected into a health mice at the same time, and the X-ray image was shown in Fig. 15, compared with iohexol, MoS₂-PEG had a stronger X-ray imaging ability, demonstrating MoS₂-PEG had a great potential as a X-ray contrast agent in vivo.

4. Conclusion

In summary, a new two-dimensional MoS₂ based multifunctional drug delivery system (MoS₂-PEG/DOX) was successfully

developed. In this study, MoS₂-PEG/DOX served not only as a tumor-targeting drug delivery system, but also as a strong photothermal agent and a powerful X-ray contrast agent. In the *in vitro* and *in vivo* studies, MoS₂-PEG did not show noticeable toxic to mice even at very high dosages. MoS₂-PEG/DOX exhibited excellent tumor-targeting efficacy, outstanding synergistic anti-cancer effect of photothermal and chemotherapy, NIR induced endosome escaping ability and X-ray imaging property, demonstrating that MoS₂-PEG/DOX had a great potential for simultaneous diagnosis and combination therapy in cancer treatment.

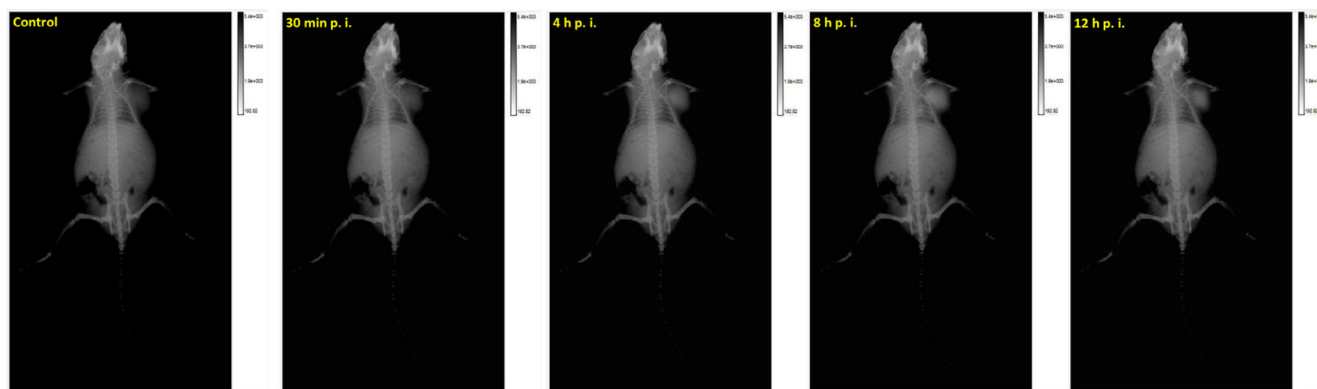


Fig. 14 – X-ray images of a tumor-bearing mouse intravenous injection of MoS₂-PEG/DOX (DOX: 10 mg/kg, MoS₂-PEG: 14.5 mg/kg) for different times.



Fig. 15 – X-ray images of a tumor-bearing mouse subcutaneous injection of MoS₂-PEG (8 mg/ml, 0.1 ml) and iohexol (240 mg/ml, 0.1 ml).

Acknowledgements

The work is supported by grants from the National Natural Science Foundation of China (Nos.81273451, 81302717 and 81101684).

Appendix: Supplementary material

Supplementary data to this article can be found online at [doi:10.1016/j.ajps.2016.12.001](https://doi.org/10.1016/j.ajps.2016.12.001).

REFERENCES

- [1] Byrne JD, Betancourt T, Brannon-Peppas L. Active targeting schemes for nanoparticle systems in cancer therapeutics. *Adv Drug Deliv Rev* 2008;60:1615–1626.
- [2] Tian Y, Jiang X, Chen X, et al. Doxorubicin-loaded magnetic silk fibroin nanoparticles for targeted therapy of multidrug-resistant cancer. *Adv Mater* 2014;26:7393–7398.
- [3] Hua MY, Yang HW, Liu HL, et al. Superhigh-magnetization nanocarrier as a doxorubicin delivery platform for magnetic targeting therapy. *Biomaterials* 2011;32:8999–9010.
- [4] Kopeček J. Smart and genetically engineered biomaterials and drug delivery systems. *Eur J Pharm Sci* 2003;20:1–16.

- [5] Nishiyama N, Okazaki S, Cabral H, et al. Novel cisplatin-incorporated polymeric micelles can eradicate solid tumors in mice. *Cancer Res* 2003;63:8977–8983.
- [6] Bitounis D, Ali-Boucetta H, Hong BH, et al. Prospects and challenges of graphene in biomedical applications. *Adv Mater* 2013;25:2258–2268.
- [7] Tian B, Wang C, Zhang S, et al. Photothermally enhanced photodynamic therapy delivered by nano-graphene oxide. *ACS Nano* 2011;5:7000–7009.
- [8] Shi J, Wang L, Zhang J, et al. A tumor-targeting near-infrared laser-triggered drug delivery system based on GO@Ag nanoparticles for chemo-photothermal therapy and X-ray imaging. *Biomaterials* 2014;35:5847–5861.
- [9] Ganatra R, Zhang Q. Few-layer MoS₂: a promising layered semiconductor. *ACS Nano* 2014;8:4074–4099.
- [10] Li H, Qi X, Wu J, et al. Investigation of MoS(2) and graphene nanosheets by magnetic force microscopy. *ACS Nano* 2013;7:2842–2849.
- [11] Liu N, Kim P, Kim JH, et al. Large-area atomically thin MoS₂ nanosheets prepared using electrochemical exfoliation. *ACS Nano* 2014;8:6902–6910.
- [12] Liu T, Wang C, Gu X, et al. Drug delivery with PEGylated MoS₂ nano-sheets for combined photothermal and chemotherapy of cancer. *Adv Mater* 2014;26:3433–3440.
- [13] Chhowalla M, Amaratunga GA. Thin films of fullerene-like MoS₂ nanoparticles with ultra-low friction and wear. *Nature* 2000;407:164–167.
- [14] Roy K, Padmanabhan M, Goswami S, et al. Graphene-MoS₂ hybrid structures for multifunctional photoresponsive memory devices. *Nat Nanotechnol* 2013;8:826–830.
- [15] Castellanos-Gomez A, van Leeuwen R, Buscema M, et al. Single-layer MoS(2) mechanical resonators. *Adv Mater* 2013;25:6719–6723.
- [16] Cheng L, Liu J, Gu X, et al. PEGylated WS(2) nanosheets as a multifunctional theranostic agent for *in vivo* dual-modal CT/photoacoustic imaging guided photothermal therapy. *Adv Mater* 2014;26:1886–1893.
- [17] Lee YT, Choi K, Lee HS, et al. Graphene versus ohmic metal as source-drain electrode for MoS(2) nanosheet transistor channel. *Small* 2014;10:2356–2361.
- [18] Teo WZ, Chng EL, Sofer Z, et al. Cytotoxicity of exfoliated transition-metal dichalcogenides (MoS₂, WS₂, and WSe₂) is lower than that of graphene and its analogues. *Chemistry (Easton)* 2014;20:9627–9632.
- [19] Okuda T, Kawakami S, Akimoto N, et al. PEGylated lysine dendrimers for tumor-selective targeting after intravenous injection in tumor-bearing mice. *J Control Release* 2006;116:330–336.
- [20] Hatakeyama H, Akita H, Harashima H. A multifunctional envelope type nano device (MEND) for gene delivery to tumours based on the EPR effect: a strategy for overcoming the PEG dilemma. *Adv Drug Deliv Rev* 2011;63:152–160.
- [21] Liu T, Wang C, Cui W, et al. Combined photothermal and photodynamic therapy delivered by PEGylated MoS₂ nanosheets. *Nanoscale* 2014;6:11219–11225.
- [22] Shi J, Wang L, Gao J, et al. A fullerene-based multi-functional nanoplatform for cancer theranostic applications. *Biomaterials* 2014;35:5771–5784.
- [23] Park W, Baik J, Kim TY, et al. Photoelectron spectroscopic imaging and device applications of large-area patternable single-layer MoS₂ synthesized by chemical vapor deposition. *ACS Nano* 2014;8:4961–4968.
- [24] Yin W, Yan L, Yu J, et al. High-throughput synthesis of single-layer MoS₂ nanosheets as a near-infrared photothermal-triggered drug delivery for effective cancer therapy. *ACS Nano* 2014;8:6922–6933.
- [25] Nelson CE, Kintzing JR, Hanna A, et al. Balancing cationic and hydrophobic content of PEGylated siRNA polyplexes enhances endosome escape, stability, blood circulation time, and bioactivity *in vivo*. *ACS Nano* 2013;7:8870–8880.
- [26] Xiang B, Dong DW, Shi NQ, et al. PSA-responsive and PSMA-mediated multifunctional liposomes for targeted therapy of prostate cancer. *Biomaterials* 2013;34:6976–6991.
- [27] Peddada LY, Harris NK, Devore DI, et al. Novel graft copolymers enhance *in vitro* delivery of antisense oligonucleotides in the presence of serum. *J Control Release* 2009;140:134–140.
- [28] Gu J, Wang X, Jiang X, et al. Self-assembled carboxymethyl poly (L-histidine) coated poly (beta-amino ester)/DNA complexes for gene transfection. *Biomaterials* 2012;33:644–658.
- [29] Farimani AB, Min K, Aluru NR. DNA base detection using a single-layer MoS₂. *ACS Nano* 2014;8:7914–7922.
- [30] Elsherbini AA, Saber M, Aggag M, et al. Laser and radiofrequency-induced hyperthermia treatment via gold-coated magnetic nanocomposites. *Int J Nanomedicine* 2011;6:2155–2165.
- [31] Wang C, Ning L, Wang H, et al. A peptide-mediated targeting gene delivery system for malignant glioma cells. *Int J Nanomedicine* 2013;8:3631–3640.
- [32] Shi J, Liu Y, Wang L, et al. A tumoral acidic pH-responsive drug delivery system based on a novel photosensitizer (fullerene) for *in vitro* and *in vivo* chemo-photodynamic therapy. *Acta Biomater* 2014;10:1280–1291.
- [33] Qu Q, Liu J, Zhou HH, et al. Nrf2 protects against furosemide-induced hepatotoxicity. *Toxicology* 2014;324:35–42.
- [34] Shin JH, Lee CW, Oh SJ, et al. Hepatoprotective effect of aged black garlic extract in rodents. *Toxicol Res* 2014;30:49–54.
- [35] Bertrand N, Wu J, Xu X, et al. Cancer nanotechnology: the impact of passive and active targeting in the era of modern cancer biology. *Adv Drug Deliv Rev* 2014;66:2–25.
- [36] Park K. Questions on the role of the EPR effect in tumor targeting. *J Control Release* 2013;172:391.